analytical chemistry

pubs.acs.org/ac Article

Smartphone-Assisted Robust Sensing Platform for On-Site Quantitation of 2,4-Dichlorophenoxyacetic Acid Using Red Emissive Carbon Dots

Dandan Su,[‖] Xiaosong Han,[‖] Xu Yan,* Rui Jin, Hongxia Li, Deshuai Kong, Hao Gao, Fangmeng Liu, Peng Sun, and Geyu Lu*

Cite This: *Anal. Chem.* 2020, 92, 12716−12724 Read Online

ACCESS | Metrics & More | Article Recommendations | Supporting Information

ABSTRACT: On-site quantitative analysis of pesticide is of significant importance for addressing serious public health issues in clinical, food, and environmental settings. Herein, we designed a novel smartphone-assisted sensing platform for on-site monitoring of 2,4-dichlorophenoxyacetic acid (2,4-D) based on carbon dots/cobalt oxyhydroxide nanosheet (CDs/CoOOH) composite. In this work, a red emissive CDs/CoOOH composite was proposed as a signal indicator for shielding background interference, enhancing anti-interference capability. 2,4-D as an inhibitor of alkaline phosphatase could specifically suppress the production of ascorbic acid, which restrained in situ etching of the CDs/CoOOH composite and further triggered the fluorescence response of the biosensor. By employing a lab-on-smartphone based device and self-designed application software, the fluorescence image was directly captured and analyzed with a sensitive detection limit of 100 μg L^{-1} for 2,4-D. Merging the CDs/CoOOH composite-based fluorometric system with the smartphone-assisted optical reader, such a cost-effective and portable platform provided a new sight for on-site monitoring of pesticide and expanded application prospect in the field of biological analysis.

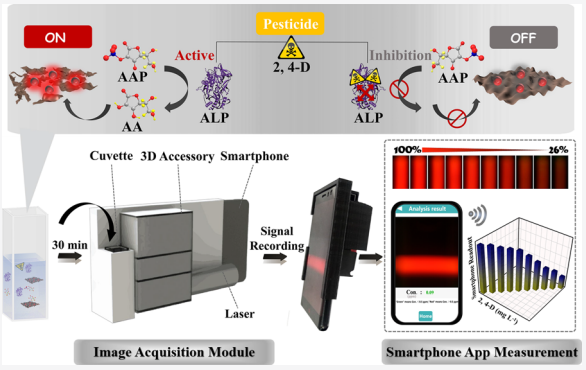

Pesticide contamination has severely attacked the ecosystem and food safety, gradually becoming an escalating threat to public health. As an auxin-type herbicide for regulating plant growth,[1] 2,4-dichlorophenoxyacetic acid (2,4-D) is considered as one of the "probably carcinogenic compound to humans" (Group 2B).[2,3] In general, 2,4-D and its derivatives possess toxicity toward numerous aquatic and mammalian species, tending to cause organ damage in thyroid, kidneys, and ovaries during their long-term exposure.[4] Experiment on species-specific pharmacokinetics has demonstrated the delayed neurobehavioral development in animals after exposure to 2,4-D.[5] Hence, accurate and efficient assessment of 2,4-D is of great significance in support of environment surveillance with increasing concern to public health and environmental quality.

The core guarantee of pollution assessment is the powerful innovation of sensing technology. Current laboratory-based pesticides-analyzing conventional apparatus, comprising chromatography,[6] mass spectrometry,[7] and enzyme-linked immunosorbent assay (ELISA),[8] can achieve identification analysis with satisfactory precision and resolution. Despite these techniques being featured with forceful ability, the operational complexity, time-consuming procedure, and requirement of sophisticated instrumentation restrain its widespread applications, especially the on-site monitoring in resource constrained or noncentralized settings.[9] In recent years, considerable endeavors have been taken to establish real-time sensing techniques for pesticide in a reliable and portable manner. The antibody-based lateral flow biosensors have so far been the popular technique according to the color change for point-of-care (POC) measurement of pesticide, assisted by visual observation.[10,11] However, these are frequently fabricated by using complicated antibody preparation technology and test strip assembly skill, which is not easy to achieve. Furthermore, these strategies are limited to qualitative identification or semiquantitative analysis, making them unsuitable for tracing target accurately owing to the obstruction of recognizing the subtle changes. Another encountered potential problem is the false-negative results caused by the need for high concen-

Received: August 3, 2020
Accepted: August 20, 2020
Published: August 20, 2020

https://dx.doi.org/10.1021/acs.analchem.0c03275
Anal. Chem. 2020, 92, 12716−12724

Scheme 1. Schematic Illustration of CDs/CoOOH Nanosheet Composite-Based Sensing Platform for 2,4-D

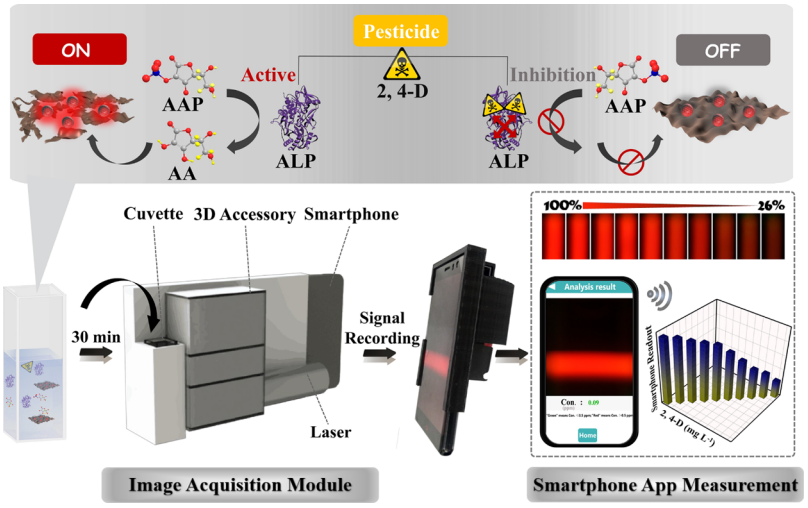

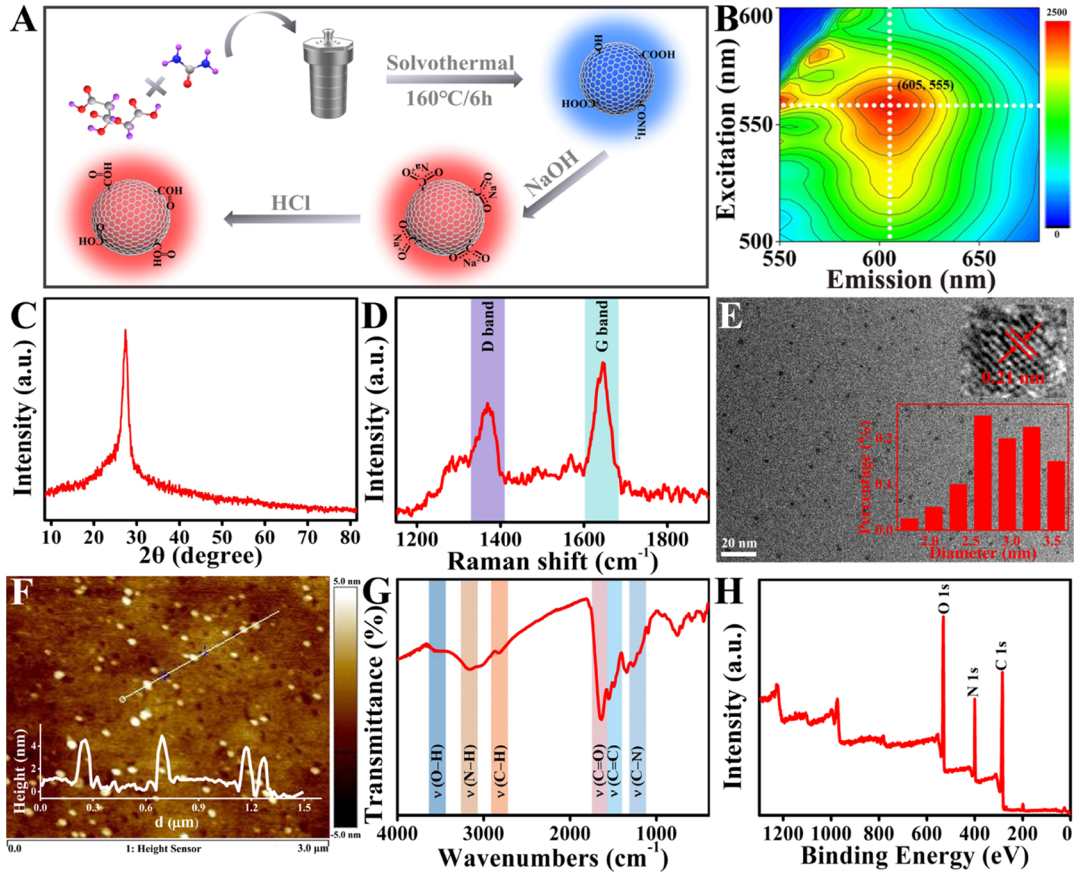

Figure 1. (A) Synthetic route of CDs; (B) contour map, (C) XRD pattern, (D) Raman spectrum, (E) TEM/HRTEM image, (F) AFM image, (G) FT-IR spectrum, and (H) XPS survey spectrum of CDs.

trations of target. Therefore, there is a lack of suitable platform to analyze pesticide for on-site assay.

With the progress of advanced nanotechnology, fluorescent nanomaterials, such as quantum dots, carbon dots (CDs), and silicon dots, have provided unique photoluminescent behaviors and sensitive responses for fabricating pesticides biosensor.[12−17] For example, our group explored a fluorometric system based on urease-controlled response of green-emissive fluorescent copper nanoclusters. By evaluating the fluorescence (FL) images captured by a smartphone, the platform revealed a lower background interference and higher contrast in comparison with colorimetry-based biosensors.[18] Following this strategy, the combination of CDs and gold nanoparticles was utilized for fabricating fluorescent assay of pesticide, achieving sensitive detection performance relying on the merit of efficient interaction of nanomaterials and high catalysis ability of enzyme.[19] However, these blue or green emissive FL probes severely suffered from autofluorescence interference of the sample matrix, causing poor repeatability and false-positive results. What is more, a smartphone with a high-resolution

https://dx.doi.org/10.1021/acs.analchem.0c03275
Anal. Chem. 2020, 92, 12716−12724

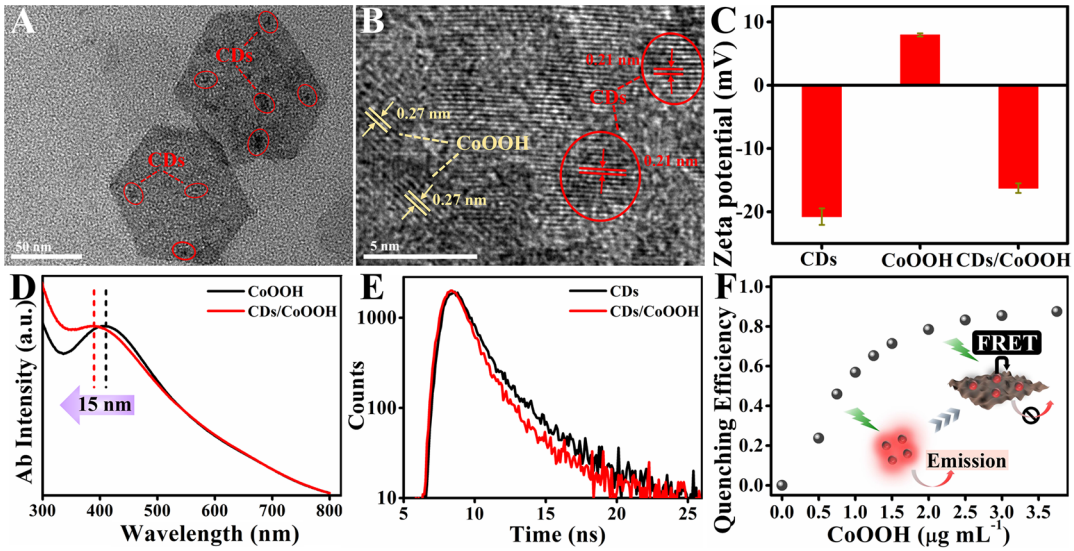

Figure 2. (A) TEM and (B) HRTEM image of CDs/CoOOH composite; (C) zeta potentials data; (D) UV−vis absorption spectra of the CoOOH nanosheets and CDs/CoOOH composite; (E) FL lifetimes of CDs and CDs/CoOOH composite; and (F) FL QE of CoOOH nanosheets.

camera working as a color shooter has been utilized to minimize the device size and simplify the process of information collection.[20,21] These platforms require computer processing software (ImageJ and MATLAB) for analyzing data, making the image processing complicated, which could not satisfy the demand of real-time monitoring.

In this case, we constructed a handheld smartphone-assisted fluorometric platform for on-site quantification of 2,4-D with excellent selectivity based on the optical features of red-emission CDs and signal amplification of alkaline phosphatase (ALP). The red emissive CDs whose maximum emission center was located at 605 nm with high stability were synthetized via one-step solvothermal treatment of citric acid and urea under *N*,*N*-dimethylformamide, which could efficaciously shield photodamage and autofluorescence interference and enhance anti-interference capability toward matrix. As shown in Scheme 1, the CDs were self-assembled on the surface of the cobalt oxyhydroxide (CoOOH) nanosheets to fabricate CDs/CoOOH composite based on electrostatic force, which resulted in FL quenching response through the Förster resonance energy transfer (FRET) mechanism. By employing the chemical reaction with ALP hydrolysate (ascorbic acid, AA), the CDs/CoOOH composite was decomposed to release CDs, causing FL recovery of the system. 2,4-D specifically inhibited the activity of ALP, which blocked the generation of AA, further inducing the FL response of the CDs/CoOOH composite. For accurate quantification, the corresponding images were captured by a smartphone, together with 3D-printed auxiliary equipment. Using a self-designed application, color intensity was directly transformed into digital information that was straightway relevant to the concentration of the analyte 2,4-D. As far as we know, there are few reports about pesticide detection based on smartphone-based 3D-printed accessory. Considering these advantages such as excellent optical properties of CDs, simplified data analysis, and easy-to-print auxiliary device, it is believed that the proposed smartphone-based handheld platform could afford experience for designing a neotype sensing strategy in pesticide monitoring.

RESULTS AND DISCUSSION

Characterization of CDs. Nitrogen-enriched CDs have been facilely synthesized via solvothermal treatment of citric acid and urea under *N*,*N*-dimethylformamide. Employing surface charge engineering, CDs were treated with sodium hydroxide and hydrochloric acid solution to achieve red emissive properties (Figure 1A). The excitation-emission matrix image of CDs was displayed in three-dimensional FL plots, supporting the optical properties with a single emission center and excitation-wavelength-dependence (Figure 1B). Note that the maximum emission wavelength was 605 nm under an excitation wavelength of 555 nm (Figure S1). The visible red character "JLU" on a common filter paper written by using CD solvent (H_2O) as ink was displayed through the 365 nm UV lamp, further demonstrating the red emission of CDs (Figure S2). The relative FL quantum yield (QY) of CDs is detailed in the Supporting Information and calculated to be 7.8% using rhodamine 6G as a reference (Figure S3). Additionally, the UV−vis spectrum exhibited an absorption peak at 546 nm illustrated large-sized conjugated sp^2-domain in CDs. As revealed in Figure 1C, XRD data exhibited a sharp peak at 27.1° that corresponded to the (002) plane of graphite structure,[22,23] indicating that the high conjugate sp^2-domain occupied major position within the core part of CDs. To identify the state of carbon, two characteristic peaks including the disordered peak at 1367 cm^{-1} (D band) and the sharp peak at 1643 cm^{-1} (G band) were obtained under 532 nm laser excitation in the Raman spectrum (Figure 1D), which displayed lattice defects and E_{2g} symmetry of the carbon atom, respectively.[24]

Morphological and dimensional characteristics of CDs were obtained by transmission electron microscopy (TEM) image (Figure 1E). The average diameter was about 2.9 ± 0.9 nm with homogeneous distribution. Together with that, distinct crystalline lattice fringes with a spacing of 0.21 nm were observed in a high-resolution TEM image (inset of Figure 1E), which coincided with the (100) plane of graphene.[25] The topographic heights (2.9−4.9 nm) of CDs in an atomic force microscopy (AFM) image (Figure 1F) demonstrated that CDs were made of 10−16 layers of graphene-like sheets. The

https://dx.doi.org/10.1021/acs.analchem.0c03275
Anal. Chem. 2020, 92, 12716−12724

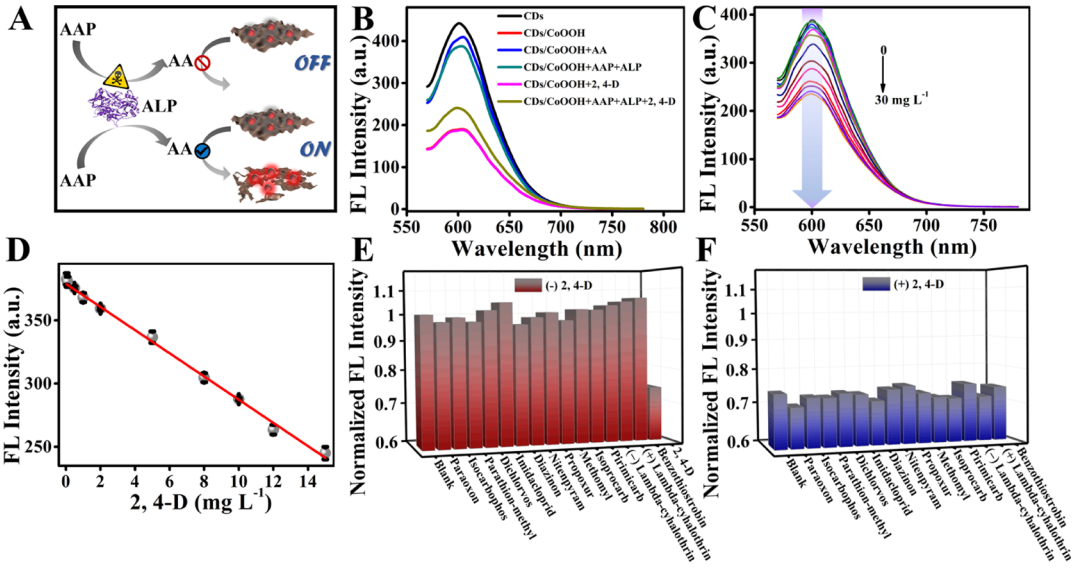

Figure 3. (A) Analysis route of 2,4-D; (B) feasibility of the sensor; (C) FL spectra with various concentrations of 2,4-D; (D) linear relationship between FL intensity and the concentration of 2,4-D; (E) selectivity; and (F) anti-interference performance studies.

characteristic absorption of functional groups including 3450 cm^{-1}, 3180 cm^{-1}, 1643 cm^{-1}, and 1273 cm^{-1} for ν (O−H), ν (N−H), ν (C═O), and ν (C−N), respectively, was shown in the Fourier transform infrared (FTIR) spectrum (Figure 1G), which corresponded to the presence of carboxyl and amino group on the surface of CDs.[26,27] Furthermore, the X-ray photoelectron spectroscopy (XPS) survey scan (Figure 1H) was utilized to quantitate the chemical structure of CDs. Three typical peaks at 285.1, 399.6, and 531.0 eV were displayed, indicating that they mainly consisted of carbon (60.61%), nitrogen (16.54%), and oxygen element (22.85%), respectively. High-resolution C 1s, N 1s, and O 1s XPS spectra in Figure S4 presented different types of C, N, and O,[28−31] which further confirmed the presence of amino N and −COOH groups. The contents of C═C/C−C, C−N, pyrrolic N, and graphitic N contributed to the π-conjugated system with a pair of p-electrons, revealing the rich sp^2-conjugated skeleton. Owing to sodium hydroxide/hydrochloric acid treatment, surface functionalization induced-increasing of carboxylate groups caused electron-rich feature of the inner surface, which was related to the red-emission characteristic of CDs. Therefore, such a red emissive wavelength might be attributed to sp^2-domain controlling and surface charge engineering, where DMF as a nitrogenous solvent endowed CDs with a large-sized conjugated sp^2 domain, and the treatment of alkaline/acid solvent could achieve surface charge engineering.[25,32,33] Physical and chemical stability is one of the significant parameters in practical applications. Note that the CDs held satisfactory stability across various harsh chemical and physical conditions (Figures S5−S9). Thus, the overall results elucidated that the red emissive CDs possessed easy preparation, rich surface carboxyl group, and excellent stability, making them promising as a signal indicator in sensing application.

Fabrication of the CDs/CoOOH Composite. The hexagonal shaped-CoOOH nanosheets with a strong wide-band absorption from 350 to 700 nm (Figures S10−S14) were employed as a promising dual-functional carrier and quencher for constructing nanocomposites.[34−36] Through electrostatic force, CDs were self-assembled on the surface of CoOOH nanosheets to fabricate the CDs/CoOOH composite. Carefully observing, crystalline lattice fringes of CDs (0.21 nm) and CoOOH nanosheets (0.27 nm) simultaneously existed in the CDs/CoOOH composite (Figure 2A,B). The binding between CDs and CoOOH nanosheets was further monitored through zeta potential measurements. Significant changes in zeta potential (−15.5 mV) after loading CDs verified the electrostatic attraction between the positively charged nanosheets (+8.0 mV) and the negatively charged CDs (−20.8 mV), which contributed to the assembly of composite materials (Figure 2C).[37] Moreover, wide-range UV−vis absorption of CoOOH nanosheets was concentrated at 408 nm, while that of CDs/CoOOH composite possessed blue-shift to 393 nm (Figure 2D), supporting the formation of the composite.

In the self-assembly CDs/CoOOH composite, CDs served as an energy donor, while CoOOH nanosheets served as an energy acceptor that could efficaciously block the FL of CDs. To understand the sensing mechanism of CoOOH-triggered FL quenching, the optical characteristic of nanomaterials was first investigated. As revealed in Figure S15, there was visible overlap between the absorption spectrum of nanosheets (black line) and the emission spectrum of CDs (red line), forming a donor−acceptor pair that resulted in the FRET mechanism or inner filter effect. Furthermore, the formation of the CDs/CoOOH composite shortened the distance between the donor and acceptor. More importantly, the quenching mechanism was investigated by exploring FL lifetime. As displayed in Figure 2E, time-resolved luminescence decay curve of the CDs/CoOOH composite (1.46 ns) was shorter than that of CDs (1.91 ns), implying that the reaction mechanism could be the FRET process.[38] As expected, the FL intensity of CDs was gradually quenched by CoOOH nanosheets (0−3.75 $\mu g\ mL^{-1}$) (Figure S16), and quenching efficiency (QE) could reach about 88% in the presence of 3.75 $\mu g\ mL^{-1}$ of CoOOH nanosheets (Figure 2F).[39,40] Such an excellent energy transfer efficiency was chiefly ascribed to the larger surface area and stronger optical absorption of CoOOH nanosheets. All abovementioned results demonstrated that the CDs/CoOOH

https://dx.doi.org/10.1021/acs.analchem.0c03275
Anal. Chem. 2020, 92, 12716−12724

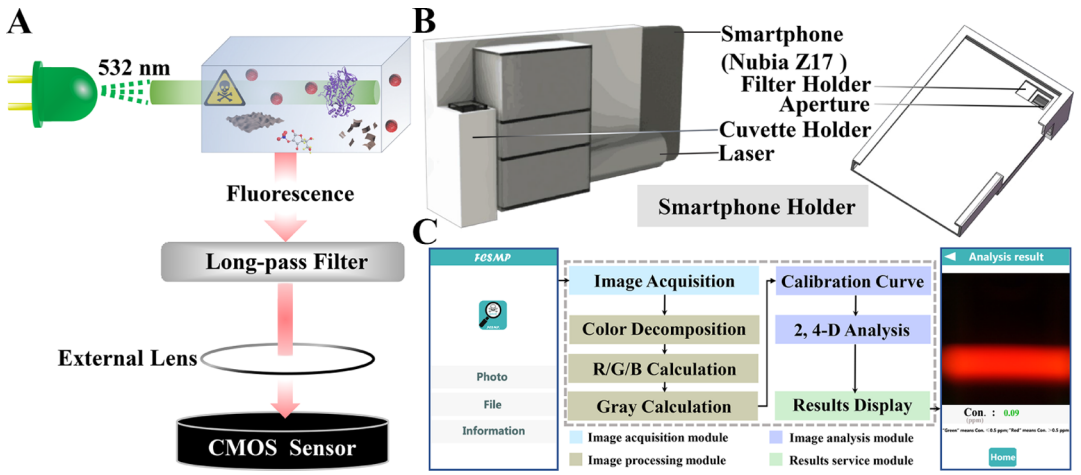

Figure 4. Hardware design of a smartphone fluorometric sensing platform: (A) optical design; (B) 3D structure design; and (C) image decomposition method for 2,4-D monitoring using a smartphone app.

composite was successfully prepared for further fabricating the biosensor.

Sensing Performance toward 2,4-D. Bestowed with the favorable feasibility of the CDs/CoOOH composite, the system was employed to accurately and reliably quantify trace-level pesticide (Figure 3A). ALP could catalytically hydrolyze ascorbic acid-2-phosphate trisodium salt (AAP) into ascorbic acid (AA) that effectively reduced CoOOH nanosheets to Co^{2+}, further controlling the degradation of the CDs/CoOOH composite (green line, Figure 3B). 2,4-D as an enzyme inhibitor could specifically suppress the activity of ALP,[41] which hindered the formation of AA and further tuned the FL intensity of the system (brown line). What is more, no significant effect on the CDs/CoOOH composite was found when adding equivalent concentration of 2,4-D individually (purple line), demonstrating the feasibility of the present strategy for profiling 2,4-D. In this sensing platform, ALP was served as antennae for selectively recognizing pesticide and catalytically hydrolyzing the substrate. Thus, the CDs/CoOOH composite was systematically investigated for the sensing performance toward ALP. Under optimal conditions (Figures S17−S19), the FL intensity obviously enhanced with the increasing of ALP from 0.1 to 7.0 U L^{-1}. As revealed in Figure S20, a good linear regression equation (R^2 = 0.990) between FL intensity and ALP concentration was F = 204.816 + 24.207 [ALP], U L^{-1}.

Taking advantage of good performance toward ALP, the CDs/CoOOH/AAP system was utilized for monitoring 2,4-D (Figure S21). As expected, along with the concentrations of 2,4-D increasing from 0 to 30 mg L^{-1}, the FL intensity at 605 nm was decreased gradually (Figure 3C). The regression equation in the range of 0.05−15 mg L^{-1} was estimated to be F = 378.964−9.173 [2,4-D], mg L^{-1} (Figure 3D), along with good fitting relationship (R^2 = 0.994). It was worth mentioning that the limit of detection (LOD) was calculated to be 10 μg L^{-1} (S/N=3), meeting the detection requirement of maximum residue limit value (GB 2763-2019) set by the National Health Commission of the People's Republic of China. Moreover, a comparison with previous approaches showed that the proposed bioassay performed well with an acceptable LOD and a linear range (Table S1). Note that the sample-to-answer analysis time (30 min) was shorter than or comparable to that of immunoassay-, chromatograph-, and enzyme-based strategies.

Specificity and anti-interference ability are significant indexes in evaluating the capacity of the enzyme-based sensor, particularly in on-site application. To simulate the actual environment, other common pesticides (organophosphorus pesticides, neonicotinoid pesticides, carbamates pesticides, and pyrethroid pesticides) and coexisting substances (metal ions, proteins, and amino acids) were chosen to evaluate the interference effect. A histogram of normalized intensity in Figures 3E and S22 exhibited that only 2,4-D induced remarkable response of the system, while other interference substance with the same concentration (10.0 mg L^{-1}) had no significant effect. Noteworthily, almost the same response to 2,4-D was obtained when the above substance coexisted in the system (Figure 3F). Compared with cholinesterase[6,42] and tyrosinase[43] that were incapable to distinguish a class of pesticides (organophosphorus pesticides and carbamate pesticides), the CDs/CoOOH/AAP/ALP system possessed high selectivity and anti-interference performance for 2,4-D detection, showing remarkable superiority among these existing enzyme-based strategies. The good selectivity and anti-interference capacity maybe attributed to the high specificity of ALP toward 2,4-D and CDs/CoOOH composite-assisted target recognition.

Such an excellent performance for sensing 2,4-D might arise from the following distinctive features: (1) The established CDs as a signal indicator exhibited red emission at 605 nm, which could conquer the influence from inevitable autofluorescence of biological matrix, efficiently blocking background interference and enhancing anti-interference capability. (2) The CoOOH nanosheets acted as a carrier and quencher toward CDs with high QE, remarkably improving the detection sensitivity of the platform. (3) The high-performance of selectivity was related to enzyme (ALP), which not only possessed high selectivity toward the substrate (AAP) but also performed specific recognition capacity to the pesticide. All above results demonstrated that the CDs/CoOOH/AAP/ALP system possessed excellent performance for monitoring 2,4-D.

Smartphone Fluorometric Sensing Platform. Current commercial apparatus could satisfy the requirements of quantitative analysis; nevertheless, the portable detection of the analyte was still restricted to the operational complexity

https://dx.doi.org/10.1021/acs.analchem.0c03275
Anal. Chem. 2020, 92, 12716−12724

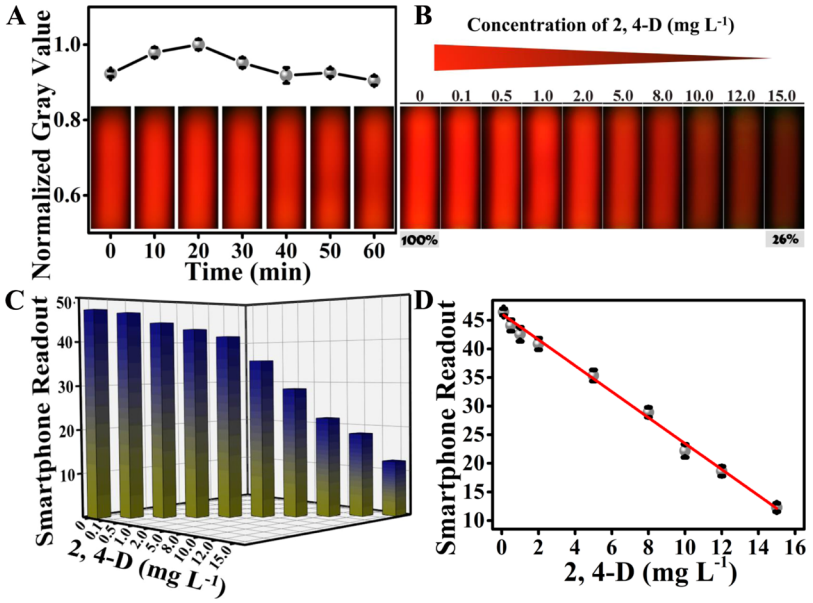

Figure 5. (A) Gray value of photographs within an hour; (B) photographs with different target concentrations; (C) smartphone readout gray value vs the concentration of 2,4-D; and (D) linear relationship between smartphone readout gray value and the concentration of 2,4-D.

and inaccessibility of laboratory-based apparatus.[44,45] Hence, it would make sense to establish integrated and man-carried equipment for pesticides quantitative analysis, in which a suitable light source and signal readout detector were of great necessity.[46,47] For this purpose, the CDs/CoOOH composite-based system was further employed to investigate the smartphone fluorometric sensing platform. For minimizing environmental factor (relative position between sample and camera and light source intensity) and operation error (information extraction and transformation), a handheld device was proposed to solve the current limitations of image-capturing instability and image-processing complexity. It mainly consisted of a 3D model accessory with the size of 120.0 × 78.0 × 34.5 mm, a 532 nm laser (Φ 20 × 60 mm), a standard cuvette (inner diameter: 10 mm), and a long-pass filter with a blocking wavelength of 590 nm (10 × 10 mm). Figures 4 and S23 show hardware design (optical, 3D structure, and actual device design) of the integrated smartphone-connected device for the Nubia Z17 smartphone. The printing material was black opaque polylactic acid polymers for preventing light penetration from surrounding environment and minimizing light leakage. During imaging, mini-laser diodes (50 mW) with a wavelength of 532 nm served as a light source of excitation powered by a 3.7 V 18650 lithium-ion battery, which was embedded into the backside baseboard of the auxiliary device. Passed through the cuvette, the transmitted light intensity was collected by a smartphone CMOS (complementary metal−oxide semiconductor) sensor. The long-pass filter that strongly attenuated shorter wavelengths was anchored in front of a smartphone camera to clear the background noise triggered by excitation light and minimize scattered excitation photons and autofluorescence, and the distance between the filter and the smartphone camera was 1.5 mm. Therefore, the compact and portable device could obtain smartphone images for quantitative sensing pesticide in a high sensitivity and low background manner. It was worth noting that the manufacturing cost of such a handheld device was as low as $20, greatly reducing the cost of an analytical platform.

Taking the data processing capacity of a smartphone into account, a custom-designed app named "Fluorescence Color Scan in Monitoring Pesticide (FCSMP)" was facilitated for the device control and data processing of 2,4-D (Figure 4C). This app software controlled the smartphone to collect a photo image, analyze the concentration-pixel retrieval, and evaluate the detection results (Figure S24). The platform possessed good stability via analyzing FL images within 60 min (Figure 5A). Given the design and exploration above, we can directly detect 2,4-D concentrations in real-time by collecting the optical image of sample. As seen in Figure 5B, the collected images brightness of the probe solution was in negative connection with 2,4-D concentrations. Coupling with FCSMP software, the smartphone readout gray values of various analyte concentrations were acquired in Figure 5C,D. The linear relationship (R^2 = 0.990) between smartphone readout gray value and the concentration of 2,4-D was I = 46.148−2.268 [2,4-D], with a LOD of 100 μg L^{-1} (S/N=3). Although weaker than the FL spectrometry method on the basis of identical system, that the integrated smartphone-connected sensor displayed comparable liner range and LOD compared with other reported methods was worth noting (Table S1). The results of 2,4-D detection demonstrated that the smartphone-assisted fluorometric sensing platform possessed a low requirement for sample volume (50 μL), rapid (30 min), and easy readouts for POC testing.

Real Sample Evaluation. The practicability of pesticides monitoring is of significance in biological monitoring and environmental evaluation. Real samples including lake water, pear juice, human urine, and serum served as research targets to verify practical applications of the smartphone-connected sensor. All these samples showed "not detected" results of 2,4-D by proposed platform. 2,4-D with various concentrations (0.1, 0.5, 1.0, 5.0 mg L^{-1}) were spiked by means of the standard addition method. Before recovery studies, 2,4-D was extracted from the real sample employing acetonitrile that cannot dissolve water-soluble interfering substances (glutathione, cysteine, dopamine, uric acid, ascorbic acid, and gallic acid), successfully blocking the influence of matrix and

https://dx.doi.org/10.1021/acs.analchem.0c03275
Anal. Chem. 2020, 92, 12716−12724

Table 1. Analysis Results of 2,4-D in Real Samples

Sample	Added ($mg\ L^{-1}$)	Smartphone-based method			UV-vis based method		
		Founded ($mg\ L^{-1}$)	Recovery (%)	RSD (%, n=3)	Founded ($mg\ L^{-1}$)	Recovery (%)	RSD (%, n=3)
Lake water	0	-	-	-	-	-	-
	0.1	0.10	100.0	1.0	-	-	-
	0.5	0.49	98.0	0.7	0.48	96.1	2.9
	1.0	0.92	92.0	0.8	1.03	103.3	1.4
	5.0	4.74	94.8	1.2	4.64	92.8	1.8
Pear juice	0	-	-	-	-	-	-
	0.1	0.09	90.0	1.2	-	-	-
	0.5	0.46	92.0	1.2	0.52	103.9	5.3
	1.0	0.91	91.0	1.7	1.09	109.2	3.6
	5.0	5.16	103.2	1.3	4.58	91.7	0.3
Human urine	0	-	-	-	-	-	-
	0.1	0.10	100.0	1.0	-	-	-
	0.5	0.49	98.0	2.2	0.50	100.0	1.4
	1.0	0.94	94.0	0.5	1.03	103.5	2.1
	5.0	4.47	89.4	1.3	5.06	101.2	0.4
Human serum	0	-	-	-	-	-	-
	0.1	0.09	90.0	1.2	-	-	-
	0.5	0.46	92.0	0.9	0.53	105.2	0.7
	1.0	0.90	90.0	3.1	0.98	97.8	2.4
	5.0	5.02	100.4	3.0	4.46	89.3	1.0

obviously improving the selectivity (Figure S25). The recovery rates of 2,4-D from samples were obtained according to the smartphone-based method and UV−vis-based analysis method (Figure S26). As revealed in Table 1, the recoveries were in the range of 89.4−103.2% with relative standard deviations lower than 3.1%. UV−vis analysis method, where it showed good relationship (R^2 = 0.970), was used to confirm the analysis accuracy of a biosensor. Overall, the proposed platform possessed a high reliability, effectually suggesting the feasibility of a smartphone-based system in complex samples and making it possible for monitoring multiple pollutants in practical application.

CONCLUSIONS

In summary, we have constructed an innovative and portable smartphone-based POC platform for precise quantification of 2,4-D in a good sensitivity and excellent selectivity manner based on the CDs/CoOOH composite. Employing the CDs/CoOOH composite as a signal indicator, a simple but potentially promising biosensor with outstanding anti-interference capability and good sensitivity has been established. The anti-interference ability was ascribed to the red emissive CDs that could shield background interference. In virtue of introducing ALP, the biosensor exhibited specific recognition capacity toward 2,4-D, endowing it with high-performance of selectivity. The proposed approach which integrated a commercial smartphone, 3D model smartphone accessory, and self-designed app into one platform simplified image processing and minimized detection device, effectively circumventing the drawback of a bulk instrument with inaccessibility in carrying and complex computer-assistant data analysis. More significantly, the sample-to-answer analysis time of the smartphone-based platform is 30 min, which was shorter than or comparable to that of the immunoassay-, chromatograph-, and enzyme-based strategies. What is more, such a smartphone optical-sensing system has been triumphantly applied to biological and environmental samples, indicating its robust performance in biological/chemical analysis. Thus, the proposed smartphone-based handheld device provided a promising platform for the on-site monitoring pesticide, possessing potential applications in environmental screening, health monitoring, and disease prevention.

EXPERIMENTAL SECTION

Synthesis of CDs. CDs were prepared in a typical method. Briefly, 1.0 g of citric acid and 2.0 g of urea were added in 10.0 mL of DMF solution. The obtained mixture reacted at 160 °C for 6 h and then cooled to room temperature. The obtained solution was mixed with NaOH aqueous (1.25 mol L^{-1}) and centrifuged at 16,000 rpm for 10 min. In the same procedure, the precipitate was washed with HCl (5.0 wt %) and deionized water, successively. The dark powder (CDs) was obtained through the freeze-drying method.

Synthesis of the CDs/CoOOH Composite. For preparation of the CDs/CoOOH composite, 5.0 mL of CDs (0.3 mg mL^{-1}) was added to 5.0 mL of CoOOH nanosheet solution (0.025 mg mL^{-1}) and stirred for 10 min. Then, the mixed solution was sonicated for 15 min and centrifuged at 6000 rpm for 10 min. The precipitate was dissolved with 10 mL of deionized water to obtain the CDs/CoOOH composite.

Smartphone-Assisted Sensing Platform for 2,4-D. For smartphone-based quantitative analysis 2,4-D, 50 μL of various concentrations of 2,4-D and 50 μL of ALP (7.0 U L^{-1}) were equilibrated at 37 °C for 10 min. Following this, 120 μL of ascorbic acid-2-phosphate trisodium salt (AAP) (100 μmol L^{-1}) containing Tris-HCl buffer was added for incubating another 10 min at 37 °C and 160 μL of CDs/CoOOH composite solution was added to the mixture. After equilibration for 10 min, the cuvette was inserted into the 3D-printed smartphone reader to obtain the FL photo under the excitation of 532 nm laser. Then, the displayed photo image was directly analyzed using an app installed on the smartphone.

https://dx.doi.org/10.1021/acs.analchem.0c03275
Anal. Chem. 2020, 92, 12716−12724

■ ASSOCIATED CONTENT

Supporting Information

The Supporting Information is available free of charge at https://pubs.acs.org/doi/10.1021/acs.analchem.0c03275.

UV−vis, FL excitation (Ex) and FL emission (Em) spectra of CDs; character "JLU" written with CDs; QY, XPS spectra, and stability of CDs; TEM, AFM, XRD, XPS, and FT-IR spectroscopy of CoOOH nanoflakes; formation mechanism of the CDs/CoOOH composite; detection of ALP; selectivity performance studies; actual device design of the smartphone fluorometric sensing platform; user interface design of the smartphone app; UV−vis-based analysis method for 2,4-D; and comparison with other methods (PDF)

■ AUTHOR INFORMATION

Corresponding Authors

Xu Yan − *State Key Laboratory of Integrated Optoelectronics, College of Electronic Science and Engineering, Jilin University, Changchun 130012, People's Republic of China;* orcid.org/0000-0003-2152-675X; Email: yanx@jlu.edu.cn

Geyu Lu − *State Key Laboratory of Integrated Optoelectronics, College of Electronic Science and Engineering, Jilin University, Changchun 130012, People's Republic of China;* orcid.org/0000-0002-7428-2456; Email: lugy@jlu.edu.cn

Authors

Dandan Su − *State Key Laboratory of Integrated Optoelectronics, College of Electronic Science and Engineering, Jilin University, Changchun 130012, People's Republic of China*

Xiaosong Han − *College of Computer Science and Technology, Jilin University, Changchun 130012, China*

Rui Jin − *State Key Laboratory of Integrated Optoelectronics, College of Electronic Science and Engineering, Jilin University, Changchun 130012, People's Republic of China*

Hongxia Li − *Department of Food Quality and Safety, College of Food Science and Engineering, Jilin University, Changchun 130062, People's Republic of China*

Deshuai Kong − *State Key Laboratory of Integrated Optoelectronics, College of Electronic Science and Engineering, Jilin University, Changchun 130012, People's Republic of China*

Hao Gao − *College of Computer Science and Technology, Jilin University, Changchun 130012, China*

Fangmeng Liu − *State Key Laboratory of Integrated Optoelectronics, College of Electronic Science and Engineering, Jilin University, Changchun 130012, People's Republic of China*

Peng Sun − *State Key Laboratory of Integrated Optoelectronics, College of Electronic Science and Engineering, Jilin University, Changchun 130012, People's Republic of China;* orcid.org/0000-0002-9509-9431

Complete contact information is available at: https://pubs.acs.org/10.1021/acs.analchem.0c03275

Author Contributions

[‖]D.S. and X.H. contributed equally to this work.

Notes

The authors declare no competing financial interest.

■ ACKNOWLEDGMENTS

X.Y. and G.L. would like to acknowledge the financial support by the National Nature Science Foundation of China (nos. 21806051, 31901777, 61831011, 61722305 and 61833006), the Natural Science Foundation of Jilin Province (20200201021JC and 20200201218JC), the Scientific and Technological "13th Five-Year Plan" Project of Jilin Provincial Department of Education (NO. JJKH20190111KJ and JJKH20201010KJ), the National Key Research and Development Program of China (no. 2016YFC0207300), and the Program for JLU Science and Technology Innovative Research Team (no. JLUSTIRT 2017TD-07).

■ REFERENCES

(1) Jaafarzadeh, N.; Ghanbari, F.; Ahmadi, M. *Chem. Eng. J.* **2017**, *320*, 436−447.

(2) Islam, F.; Wang, J.; Farooq, M. A.; Khan, M. S. S.; Xu, L.; Zhu, J.; Zhao, M.; Muños, S.; Li, Q. X.; Zhou, W. *Environ. Int.* **2018**, *111*, 332−351.

(3) Wang, H.; Xu, Q.; Wang, J.; Du, W.; Liu, F.; Hu, X. *Biosens. Bioelectron.* **2018**, *100*, 105−114.

(4) Wang, Y.; Zeinhom, M. M. A.; Yang, M.; Sun, R.; Wang, S.; Smith, J. N.; Timchalk, C.; Li, L.; Lin, Y.; Du, D. *Anal. Chem.* **2017**, *89*, 9339−9346.

(5) Bortolozzi, A.; Duffard, R.; Antonelli, M.; Duffard, A. M. E. *Ann. N.Y. Acad. Sci.* **2006**, *965*, 314−323.

(6) Wu, Y.; Jiao, L.; Xu, W.; Gu, W.; Zhu, C.; Du, D.; Lin, Y. *Small* **2019**, *15*, 1900632.

(7) Rajski, Ł.; Martínez-Bueno, M. J.; Ferrer, C.; Fernández-Alba, A. R. *TrAC, Trends Anal. Chem.* **2019**, *118*, 587−596.

(8) Li, Y.-F.; Sun, Y.-M.; Beier, R. C.; Lei, H.-T.; Gee, S.; Hammock, B. D.; Wang, H.; Wang, Z.; Sun, X.; Shen, Y.-D.; Yang, J.-Y.; Xu, Z.-L. *TrAC, Trends Anal. Chem.* **2017**, *88*, 25−40.

(9) Chen, T.; Xu, Y.; Peng, Z.; Li, A.; Liu, J. *Anal. Chem.* **2017**, *89*, 2065−2072.

(10) Yan, X.; Song, Y.; Wu, X.; Zhu, C.; Su, X.; Du, D.; Lin, Y. *Nanoscale* **2017**, *9*, 2317−2323.

(11) Chang, J.; Li, H.; Hou, T.; Li, F. *Biosens. Bioelectron.* **2016**, *86*, 971−977.

(12) Bartelmess, J.; Quinn, S. J.; Giordani, S. *Chem. Soc. Rev.* **2015**, *44*, 4672−4698.

(13) Aragay, G.; Pino, F.; Merkoçi, A. *Chem. Rev.* **2012**, *112*, 5317−5338.

(14) Xu, G.; Zeng, S.; Zhang, B.; Swihart, M. T.; Yong, K.-T.; Prasad, P. N. *Chem. Rev.* **2016**, *116*, 12234−12327.

(15) Zhi, B.; Yao, X.; Cui, Y.; Orr, G.; Haynes, C. L. *Nanoscale* **2019**, *11*, 20411−20428.

(16) Li, M.; Chen, T.; Gooding, J. J.; Liu, J. *ACS Sens.* **2019**, *4*, 1732−1748.

(17) Song, Z.; Quan, F.; Xu, Y.; Liu, M.; Cui, L.; Liu, J. *Carbon* **2016**, *104*, 169−178.

(18) Kong, D.; Jin, R.; Wang, T.; Li, H.; Yan, X.; Su, D.; Wang, C.; Liu, F.; Sun, P.; Liu, X.; Gao, Y.; Ma, J.; Liang, X.; Lu, G. *Biosens. Bioelectron.* **2019**, *145*, 111706.

(19) Wu, X.; Song, Y.; Yan, X.; Zhu, C.; Ma, Y.; Du, D.; Lin, Y. *Biosens. Bioelectron.* **2017**, *94*, 292−297.

(20) Lee, K.-L.; You, M.-L.; Tsai, C.-H.; Lin, E.-H.; Hsieh, S.-Y.; Ho, M.-H.; Hsu, J.-C.; Wei, P.-K. *Biosens. Bioelectron.* **2016**, *75*, 88−95.

(21) Cheng, N.; Song, Y.; Fu, Q.; Du, D.; Luo, Y.; Wang, Y.; Xu, W.; Lin, Y. *Biosens. Bioelectron.* **2018**, *117*, 75−83.

(22) Zeng, L.; Li, X.; Fan, S.; Li, J.; Mu, J.; Qin, M.; Wang, L.; Gan, G.; Tadé, M.; Liu, S. *Nanoscale* **2019**, *11*, 4428−4437.

(23) Shin, J.; Guo, J.; Zhao, T.; Guo, Z. *Small* **2019**, *15*, 1900296.

(24) Kokorina, A. A.; Prikhozhdenko, E. S.; Tarakina, N. V.; Sapelkin, A. V.; Sukhorukov, G. B.; Goryacheva, I. Y. *Carbon* **2018**, *127*, 541−547.

(25) Qu, S.; Zhou, D.; Li, D.; Ji, W.; Jing, P.; Han, D.; Liu, L.; Zeng, H.; Shen, D. *Adv. Mater.* **2016**, *28*, 3516−3521.

(26) Geng, X.; Sun, Y.; Li, Z.; Yang, R.; Zhao, Y.; Guo, Y.; Xu, J.; Li, F.; Wang, Y.; Lu, S.; Qu, L. *Small* **2019**, *15*, No. e1901517.

(27) Liu, H.; Yang, J.; Li, Z.; Xiao, L.; Aryee, A. A.; Sun, Y.; Yang, R.; Meng, H.; Qu, L.; Lin, Y.; Zhang, X. *Anal. Chem.* **2019**, *91*, 9259−9265.
(28) Zhi, B.; Gallagher, M. J.; Frank, B. P.; Lyons, T. Y.; Qiu, T. A.; Da, J.; Mensch, A. C.; Hamers, R. J.; Rosenzweig, Z.; Fairbrother, D. H.; Haynes, C. L. *Carbon* **2018**, *129*, 438−449.
(29) Jiang, K.; Sun, S.; Zhang, L.; Lu, Y.; Wu, A.; Cai, C.; Lin, H. *Angew. Chem., Int. Ed.* **2015**, *54*, 5360−5363.
(30) Jiang, K.; Wang, Y.; Cai, C.; Lin, H. *Adv. Mater.* **2018**, *30*, 1800783.
(31) Jiang, K.; Gao, X.; Feng, X.; Wang, Y.; Li, Z.; Lin, H. *Angew. Chem., Int. Ed.* **2020**, *59*, 1263−1269.
(32) Li, D.; Jing, P.; Sun, L.; An, Y.; Shan, X.; Lu, X.; Zhou, D.; Han, D.; Shen, D.; Zhai, Y.; Qu, S.; Zboril, R.; Rogach, A. L. *Adv. Mater.* **2018**, *30*, 1705913.
(33) Miao, X.; Qu, D.; Yang, D.; Nie, B.; Zhao, Y.; Fan, H.; Sun, Z. *Adv. Mater.* **2018**, *30*, 1704740.
(34) Meng, H.-M.; Zhang, X.-B.; Yang, C.; Kuai, H.; Mao, G.-J.; Gong, L.; Zhang, W.; Feng, S.; Chang, J. *Anal. Chem.* **2016**, *88*, 6057−6063.
(35) Li, G.; Kong, W.; Zhao, M.; Lu, S.; Gong, P.; Chen, G.; Xia, L.; Wang, H.; You, J.; Wu, Y. *Biosens. Bioelectron.* **2016**, *79*, 728−735.
(36) Feng, L.-L.; Wu, Y.-X.; Zhang, D.-L.; Hu, X.-X.; Zhang, J.; Wang, P.; Song, Z.-L.; Zhang, X.-B.; Tan, W. *Anal. Chem.* **2017**, *89*, 4077−4084.
(37) Geng, X.; Sun, Y.; Guo, Y.; Zhao, Y.; Zhang, K.; Xiao, L.; Qu, L.; Li, Z. *Anal. Chem.* **2020**, *92*, 7940−7946.
(38) Haynes, E. P.; Rajendran, M.; Henning, C. K.; Mishra, A.; Lyon, A. M.; Tantama, M. *Anal. Chem.* **2019**, *91*, 8466−8475.
(39) Liu, J.; Tang, D.; Chen, Z.; Yan, X.; Zhong, Z.; Kang, L.; Yao, J. *Biosens. Bioelectron.* **2017**, *94*, 271−277.
(40) Zhang, L.; Qin, J.; Yang, Q.; Wei, S.; Yang, R. *Microchim. Acta* **2019**, *186*, 368.
(41) Arduini, F.; Cinti, S.; Caratelli, V.; Amendola, L.; Palleschi, G.; Moscone, D. *Biosens. Bioelectron.* **2019**, *126*, 346−354.
(42) Wu, Y.; Jiao, L.; Luo, X.; Xu, W.; Wei, X.; Wang, H.; Yan, H.; Gu, W.; Xu, B. Z.; Du, D.; Lin, Y.; Zhu, C. *Small* **2019**, *15*, 1903108.
(43) Yan, X.; Li, H.; Zheng, W.; Su, X. *Anal. Chem.* **2015**, *87*, 8904−8909.
(44) Dutta, S. *TrAC, Trends Anal. Chem.* **2019**, *110*, 393−400.
(45) Zhang, Y.; Zhao, J.; Sun, X.; Pan, W.; Yu, G.; Wang, J. *Sens. Actuators, B* **2018**, *273*, 1833−1842.
(46) Jian, D.; Wang, B.; Huang, H.; Meng, X.; Liu, C.; Xue, L.; Liu, F.; Wang, S. *Biosens. Bioelectron.* **2019**, *143*, 111632.
(47) Ding, X.; Mauk, M. G.; Yin, K.; Kadimisetty, K.; Liu, C. *Anal. Chem.* **2019**, *91*, 655−672.

https://dx.doi.org/10.1021/acs.analchem.0c03275
Anal. Chem. 2020, 92, 12716−12724